PAPER

Check for updates

Adsorption of cationic/anionic dyes and endocrine disruptors by yeast/cyclodextrin polymer composites†

Zhikun Lv,[a] Zhaoyang Wang,[a] Huaiguang Wang,[a] Jianbin Li [ID] *[abc] and Kai Li*[abc]

Factory and natural wastewaters contain a wide range of organic pollutants. Therefore, multifunctional adsorbents must be developed that can purify wastewater. Phytic acid-cross-linked Baker's yeast cyclodextrin polymer composites (IBY-PA-CDP) were prepared using a one-pot method. IBY-PA-CDP was used to adsorb methylene blue (MB), bisphenol A (BPA), and methyl orange (MO). Studies on the ionic strength and strongly acidic ion salts confirmed that IBY-PA-CDP adsorbs MO through hydrophobic interactions. This also shows that Na^+ was the direct cause of the increased MO removal. Adsorption studies on binary systems showed that MB/MO inhibited the adsorption of BPA by IBY-PA-CDP. The presence of MB increased the removal rate of MO by IBY-PA-CDP due to the bridging effect. The Langmuir isotherm model calculated the maximum adsorption capacities for MB and BPA to be 630.96 and 83.31 mg g^{-1}, respectively. However, the Freundlich model is more suitable for fitting the experimental data for MO adsorption. To understand the rate-limiting stage of adsorption, a mass-transfer mechanism model was employed. The fitting results show that adsorption onto the active sites is the rate-determining step. After five regeneration cycles, IBY-PA-CDP could be reused with good stability and recyclability.

1. Introduction

The current increase in human demand for industrial chemicals has led to rapid social development and a substantial increase in living standards; however, it has led to some adverse impacts. For example, the discharge of large quantities of pollutants into aquatic environments depletes the quality of water resources.[1] Dyes are important sources of water pollution and are produced by textile, paper, rubber, leather, plastic, and printing industries.[2] Textile mills are among the largest industrial sectors in terms of dye use and water consumption.[3] Over 700 000 tons of artificial dyes are manufactured annually, of which 10–15% is discharged into wastewater.[4] Dyes are mainly categorized as cationic (e.g., methylene blue [MB]) and anionic (e.g., methyl orange [MO]) based on the electrical properties of the molecules.[5,6] Both dyes have several applications in printing and research laboratories. Meanwhile, additives with endocrine-disrupting effects (e.g., bisphenol A [BPA]) are employed during dyeing to prevent

oxidation and degradation of textiles.[7] Dyes in industrial wastewater degrade water quality and cause toxicity, causing the death of aquatic life and human diseases.[8] Endocrine disruptors may also be carcinogenic at very low concentrations, and can cause hormonal imbalances.[9] Therefore, these dyes and endocrine disruptors must be removed from wastewater.

Adsorption has been used to purify wastewater owing to advantages such as simple operation, low energy consumption, low susceptibility to secondary pollution, and use of regenerable adsorbents.[10] Wastewater dyes or phenolic chemicals can be removed using natural biomass as an adsorbent.[11,12] Yeast is an inexpensive, readily available raw material and environmentally friendly biosorbent.[13] Yeast cell walls contain many functional groups, such as carboxyl, amino, and hydroxyl groups, and yeast has been used to treat pollutants in water, such as phenol,[14] Congo red,[13] acid orange 7,[15] and reactive red 11.[16] However, yeast has drawbacks such as low adsorption efficiency, tendency to disperse in water, and difficulty in recollection from aqueous solutions after adsorption, that limits its applications in wastewater treatment.[17] Therefore, the yeast must be modified to address these issues. Fortunately, the numerous functional groups (carboxyl, amino, and hydroxyl groups) present on its surface facilitate its ability to be chemically modified. Duan et al.[18] prepared an insoluble polymer by grafting β-cyclodextrin (β-CD) onto the surface of Baker's yeast, using thiomalic acid as a crosslinker. Liu et al.[19] prepared phosphate-modified Baker's yeast (PMBY). The maximum

[a] College of Light Industry and Food Engineering, Guangxi University, Nanning 530004, Guangxi, China. E-mail: lijb0771@sina.com; gxlikai@gxu.edu.cn; Tel: +86 13978609908; +86 13877115103

[b] Provincial and Ministerial Collaborative Innovation Center for Sugar Industry, Nanning 530004, China

[c] Engineering Research Center for Sugar Industry and Comprehensive Utilization, Ministry of Education, Nanning 530004, China

adsorption capacity of Pb^{2+} on PMBY was found to be 92 mg g^{-1}, which was about three times that of the pristine Baker's yeast.

Phytic acid (PA) is a naturally occurring cyclic organic acid and a non-toxic polymeric organic compound containing six phosphate groups and 12 hydroxyl groups. Owing to the six phosphate groups in its molecular structure, PA can be used as a cross-linking agent. In addition, this highly negatively charged chemical can enhance adsorption through electrostatic interactions with dyes or metal ions.[20] You et al.[21] modified wheat straw (WS) with PA to improve adsorption capacity for MB. The maximum adsorption quantity of PA-WS for MB was up to 205.4 mg g^{-1} at 25 °C. Bouaouina et al.[22] modified carob waste using phytic acid. Adsorption capacity of Cr(VI) increased from 243.9 to 434.8 mg g^{-1} after modification. These results showed that the adsorption capacity could be greatly improved using a PA-cross-linked adsorbent.

β-CD is a macrocyclic oligosaccharide comprising seven glucose units with a truncated cone cavity shape.[23] β-CD is of interest because of its natural nontoxicity, hydrophobic cavity, hydrophilic outer wall, and the numerous hydroxyl groups outside the macrocycle. The size of the dye is larger than the cavity of the β-CD, therefore only a part of the dye molecule can be accommodated within the cavity.[24] Furthermore, the cavities of multiple CDs create a macromolecular network, which enables the diffusion of dye molecules into the porous structure.[25] These properties promote the formation of host–guest complexes or inclusion complexes, allowing them to trap specific organic molecules.[26] This makes β-CD a potentially viable option for removing various organic micropollutants. Because natural β-CD is water-soluble, it must be converted into a water-insoluble material using a linker. Zhou et al.[27] prepared β-CD/activated carbon hydrogels by mixing β-CD with epichlorohydrin and activated carbon powder. The maximum adsorption capacity of MB can reach 166.67 mg g^{-1}. Alsbaiee et al.[28] reported a porous β-CD polymer by using rigid tetrafluoroterephthalonitrile as the crosslinker, and obtained maximum adsorption capacity toward BPA can achieve at 88 mg g^{-1}. Qiu et al.[29] grafted acrylamide and 2-acrylamido-2-methylpropane sulfonic acid onto β-CD to prepare a novel hydrogel with high adsorption capacity for MB. β-CD-based adsorbents are often prepared using toxic and carcinogenic compounds as cross-linking or grafting agents. Additionally, some adsorbents can be complicated to prepare and require a large number of organic reagents.[30] Thus, this study presents the synthesis of a new adsorbent through a simple one-step process using an eco-friendly cross-linking agent.

Currently, researchers have developed many adsorbents for removing single pollutants such as anionic, cationic dyes or nonionic endocrine disruptors. However, aqueous solutions in natural environments are mixed solutions containing various contaminants. This results in narrow application range for most adsorbents. Therefore, it is necessary to develop new multifunctional adsorbents for the simultaneous removal of anionic, cationic dyes, and nonionic endocrine disruptors.

Herein, a novel Baker's yeast-cyclodextrin polymer (IBY-PA-CDP) composite was developed. MB, MO, and BPA were used to represent cationic, anionic dyes, and nonionic endocrine disruptors, respectively. Then the adsorption properties and

mechanisms of MB, MO, and BPA were investigated using batch adsorption experiments, binary pollutant systems, mathematical modeling, and Fourier infrared spectroscopy (FTIR)/X-ray photoelectron spectroscopy (XPS) characterization. This study provides ideas for the simultaneous removal of cationic, anionic, and nonionic organic contaminants.

2. Materials and methods

2.1 Materials and reagents

Baker's yeast was obtained from Hubei Angel Yeast Co., Ltd. β-Cyclodextrin (β-CD, purity >97%) was purchased from Beijing Soleberg Technology Co., Ltd. Phytic acid (PA, 70% in H$_2$O) was obtained from Shanghai Aladdin Biochemical Technology Co., Ltd. BPA (λ_{max} = 276 nm) and humic acid (HA, purity ≥90%) were purchased from Shanghai Maclin Biochemical Technology Co., Ltd. Methylene blue (MB, λ_{max} = 665 nm), cobalt chloride hexahydrate (CoCl$_2$·6H$_2$O), methyl orange (MO, λ_{max} = 464 nm), and copper chloride dihydrate (CuCl$_2$·2H$_2$O) were obtained from Tianjin Aupsheng Chemical Co., Ltd. Manganese chloride tetrahydrate (MnCl$_2$·4H$_2$O) and sodium acetate (CH$_3$COONa) were purchased from Tianjin Kemao Chemical Reagent Co. Ltd. Methanol (CH$_3$OH) and anhydrous ethanol (C$_2$H$_5$OH) were purchased from Tianjin Komeo Chemical Reagent Co., Ltd. All reagents were of analytical grade.

2.2 Preparation of IBY

Ten grams of dry Baker's yeast was weighed and added to 100 mL of deionized water. The mixture was incubated at room temperature with shaking at 140 rpm for 15 min. The yeast solution was then inactivated in an autoclave (121 °C for 20 min). The inactivated yeast solution was centrifuged at 4000 rpm for 10 min and washed thrice. Cyclic washing was performed to separate impurities from the yeast surface to avoid any influence on the experiment. The inactivated Baker's yeast (IBY) was lyophilized and stored.
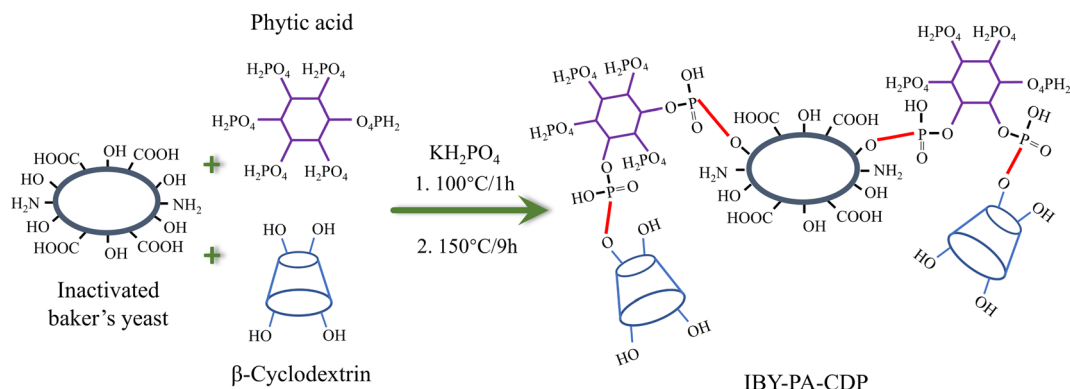
2.3 Synthesis of IBY-PA-CDP

According to researcher previously reported work with minor modification,[21] the modified IBY using PA and β-CD (IBY-PA-CDP) was synthesized via esterification as shown in Scheme 1. First, 1 g, 3.97 g, 7.09 g, and 0.56 g of IBY, PA, β-CD, and KH$_2$PO$_4$ respectively were added to deionized water and stirred at 100 °C for 1 h. Then the solutions were placed in an electrically heated desiccator at 150 °C for 9 h. The resulting product was placed in 200 mL of 0.1 mol per L NaOH solution and stirred at room temperature for 2 h. The product was washed with deionized water until the pH of the filtrate was neutral. The product was then placed in a vacuum oven at 55 °C overnight to obtain IBY-PA-CDP biomass adsorbent.

3. Results and discussion

3.1 Sample characterization

3.1.1 FTIR and XRD analysis. The surface functional groups of β-CD, IBY, and IBY-PA-CDP were detected using FTIR spectroscopy. As shown in Fig. 1a, the absorption peaks of β-CD

Scheme 1 The synthetic diagram of IBY-PA-CDP.

at 1641 and 1035 cm^{-1} are associated with the –OH bending vibration and C–OH stretching vibration, respectively. The absorption peaks at 1163 and 939 cm^{-1} correspond to the C–O–C stretching vibration and R-1, 4-bond vibration of β-CD, respectively.[31] The peaks at 1643, 1538, and 1241 cm^{-1} were observed as amide I, II, and III bands, respectively, which are the characteristic N–H vibrational peaks of yeast cell proteins.[32] The absorption peaks at 1064 cm^{-1} and 1391 cm^{-1} correspond to P=O in –OPO$_3^{2-}$ (phosphoryl) on the IBY surface and C=O stretching of the protein carboxyl group, respectively.[33] The

adsorption band of IBY-PA-CDP at –OH (3400 cm^{-1}) was reduced compared to those of β-CD and IBY, suggesting that the –OH group of IBY or β-CD reacts with PA.[31] The adsorption band of IBY-PA-CDP at 1632 cm^{-1} was the overlapping peak of the hydroxyl group bending vibration of β-CD and the amide I band of IBY. The new peak at 1703 cm^{-1} corresponds to the –OH bending vibration of the phosphate group in PA.[21] The absorption peaks at 1228 cm^{-1} was the overlapping peak of the stretch vibrations of amide III band in IBY and P=O bonds in PA. A broader new peak at 933 cm^{-1} (P–O–C) was also observed,
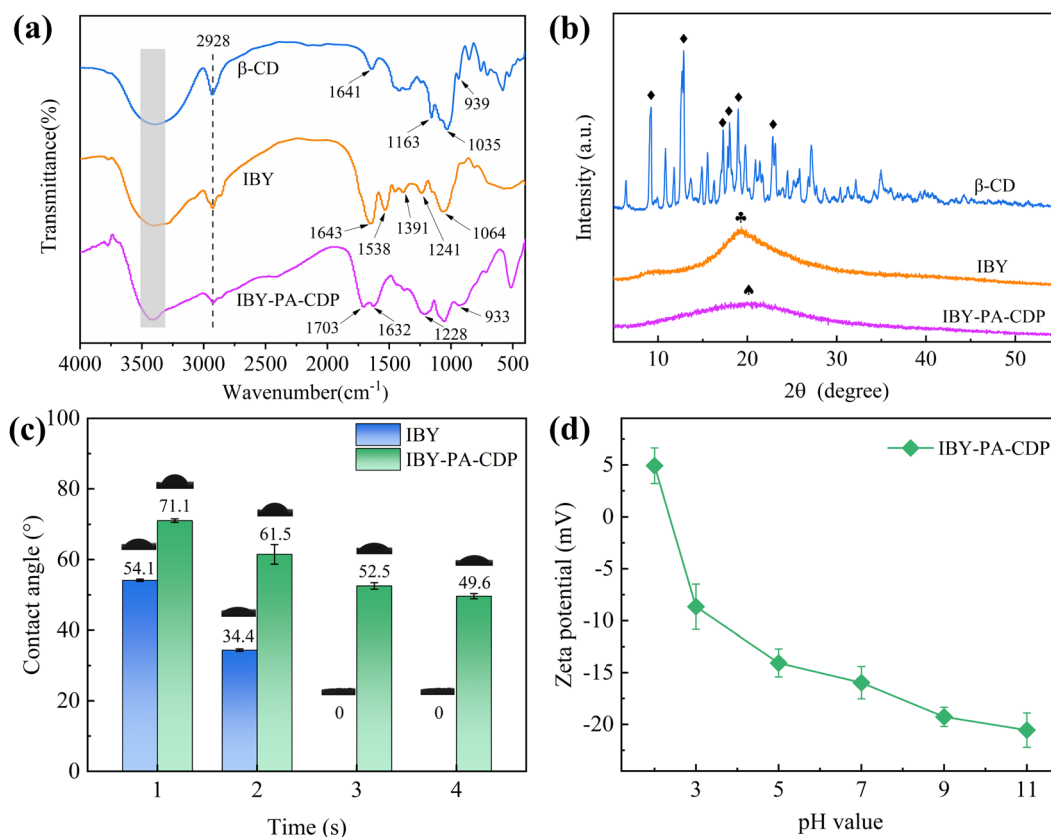

Fig. 1 (a) FTIR spectra of β-CD, IBY, and IBY-PA-CDP; (b) XRD diagrams of β-CD, IBY, and IBY-PA-CDP; (c) contact angles determined for IBY, and IBY-PA-CDP; (d) zeta potential of IBY-PA-CDP varies with pH.

which was attributed to esterification of the phosphate group on PA with the hydroxyl group on IBY and β-CD.[34,35] Then the chemical structures of IBY-PA-CDP before and after loading MB/BPA/MO were analyzed by FTIR spectroscopy in the ESI† file of the manuscript.

XRD was used to analyze the crystallographic features of the surface of the target material. The surface XRD patterns (diffraction angle 2θ) of β-CD, IBY, and IBY-PA-CDP are shown in Fig. 1b. Sharp and intense peaks are observed in the XRD patterns of β-CD, with the strongest diffraction angles (2θ): 9.21°, 12.85°, 17.27°, 17.99°, 18.97°, 23.13° (icon (♦)), which are characteristic peaks of β-CD. This confirmed the nature of the crystal structure. In contrast, IBY shows a broad peak at 2θ of 19.33° (icon (♣)). This is a characteristic of noncrystalline structures.[33] The observation of a broad peak at 20.01° (icon (♠)) in IBY-PA-CDP indicates that it is amorphous. The broad peaks in the amorphous phase were deflected owing to the cross-linking reactions of β-CD, IBY, and PA.[36] However, this is an additional advantage of this method. This is because the amorphous region of the adsorbent favors the adsorption of target compounds.[37]

3.1.2 Contact angle and zeta potential measurement. The surface hydrophobicity of the adsorbent material affects the adsorption performance of target pollutants.[38] Therefore, the hydrophobic properties of IBY and IBY-PA-CDP were examined, and their contact angles were measured. As shown in Fig. 1c, the contact angle of IBY decreased from 71.1° to 49.6° in 4 s, and that of IBY-PA-CDP decreased from 54.1° to 0° in 3 s. Although Baker's yeast cells were easily dispersed in aqueous solutions, their surfaces were still hydrophobic to a certain extent. Proteins with nonpolar structural domains and lipophosphatidic on the cell surface are crucial for preserving the hydrophobicity of the cell surface.[39,40] Unlike the original IBY (54.1°), the static water contact angle of the IBY-PA-CDP was 71.1°. The increase in the static water contact angle is also attributed to the hydrophobic inner cavity of β-CD molecules.[41] The higher the contact angle of the adsorbent, the more its hydrophobicity. After 40 s, the contact angle of the IBY-PA-CDP reached 27.3° (Fig. S2†). This demonstrates the stronger hydrophobicity of IBY-PA-CDP compared to that of IBY.

As shown in Fig. 1d, the pH increases from 2 to 11, while the zeta potential of the IBY-PA-CDP surface decreases from 4.92 mV to −20.55 mV. The zeta potential of IBY-PA-CDP was positive at pH 2. Baker yeast cell walls contain various functional groups, including carboxyl, amide, amino, and phosphate groups.[42] Therefore, IBY-PA-CDP contained amide and amino groups that were positively charged when protonated under strongly acidic conditions. However, the zeta potential of IBY-PA-CDP was negative at pH > 3. This is because IBY-PA-CDP introduced a large number of phytate molecules with phosphate groups that underwent deprotonation.[43] The higher the pH, the more negative the charge on the surface of IBY-PA-CDP.

3.1.3 SEM–EDX analysis. Photographs of IBY and IBY-PA-CDP are shown in Fig. S3.† IBY features a pale yellow surface, whereas the IBY-PA-CDP surface is black owing to PA and β-CD grafting. Fig. 2a, b and c, d show topographic images of IBY and IBY-PA-CDP, respectively, characterized by SEM at different

magnifications. IBY has a diameter range of 3–4 μm and exhibits an ellipsoidal sphere shape with a smooth and translucent layer. Owing to the chemical cross-linking between IBY, PA, and β-CD, the synthesized IBY-PA-CDP is a tightly bound substance with an irregular block structure. This solves the problems of poor mechanical strength, small size, and easy dispersion in water of Baker's yeast as a biomass adsorbent.The surface of IBY-PA-CDP is rough and uneven with tiny pores. High roughness can enhance the friction between the adsorbent and the adsorbent, which is favorable for the adsorbent to contact the binding sites.[44] The pores of IBY-PA-CDP can increase the surface area, expose active sites, and effectively accelerate the adsorption of target pollutants.[6]

The elemental mapping images of IBY and IBY-PA-CDP in Fig. 2e confirm that the four elements were uniformly distributed on the surfaces of IBY and IBY-PA-CDP. The weight percentage of each element in the samples before and after adsorption was recorded, and the data are presented in Table S1.† The elemental weight percentages showed an increase in the O and P contents on the surface of IBY-PA-CDP, indicating the successful cross-linking of β-CD and PA to the IBY surface. Based on the results for the IBY-PA-CDP model pollutants, the S weight percentages of IBY-PA-CDP/MB and IBY-PA-CDP/MO reached 1.97% and 0.13%, respectively. The weight percentage of O in IBY-PA-CDP/BPA increased by 5.51%. These results further demonstrate the effectiveness of IBY-PA-CDP in adsorbing the modeled pollutants.

3.2 Batch adsorption studies

3.2.1 Effect of initial pH. As shown in Fig. 3a and c, the equilibrium adsorption capacities for MB and MO are positively correlated with alkalinity and acidity, respectively. The adsorption capacity of IBY and IBY-PA-CDP at pH 11 for MB reached 71.29 mg g^{-1} and 563.52 mg g^{-1}. The carboxyl, hydroxyl, and phosphate groups on the surface of IBY contributed to its MB adsorption capacity. Owing to the introduction of a large number of phosphate groups into IBY-PA-CDP *via* phytate, IBY-PA-CDP exhibited higher adsorption than IBY at all pH values. No significant change was observed in the adsorption of BPA by IBY or IBY-PA-CDP at pH = 1–9 (Fig. 3b). However, a sharp decrease in BPA removal efficiency was observed at pH 11. The solution pH is higher than the acid dissociation constant of BPA ($pK_a = 10.3$) and the hydroxyl group of BPA is deprotonated.[37] Deprotonated hydroxyl groups interfere with the formation of inclusion complexes with β-CD cavities. In addition, the negatively charged IBY and IBY-PA-CDP electrostatically repelled deprotonated BPA.[45] As expected (Section 3.1.2), IBY-PA-CDP adsorbed BPA more strongly than IBY did. Fig. 3c shows that IBY can adsorb MO under acidic conditions, and the modification of β-CD increased MO adsorption. Amino or amide groups were present on the surfaces of IBY and IBY-PA-CDP (Section 3.1.1). These functional groups are protonated under acidic conditions and adsorb MO with sulfonic acid groups *via* electrostatic interactions. Although the adsorption of the MO dye by IBY-PA-CDP gradually decreased at pH 2–11, it remained above
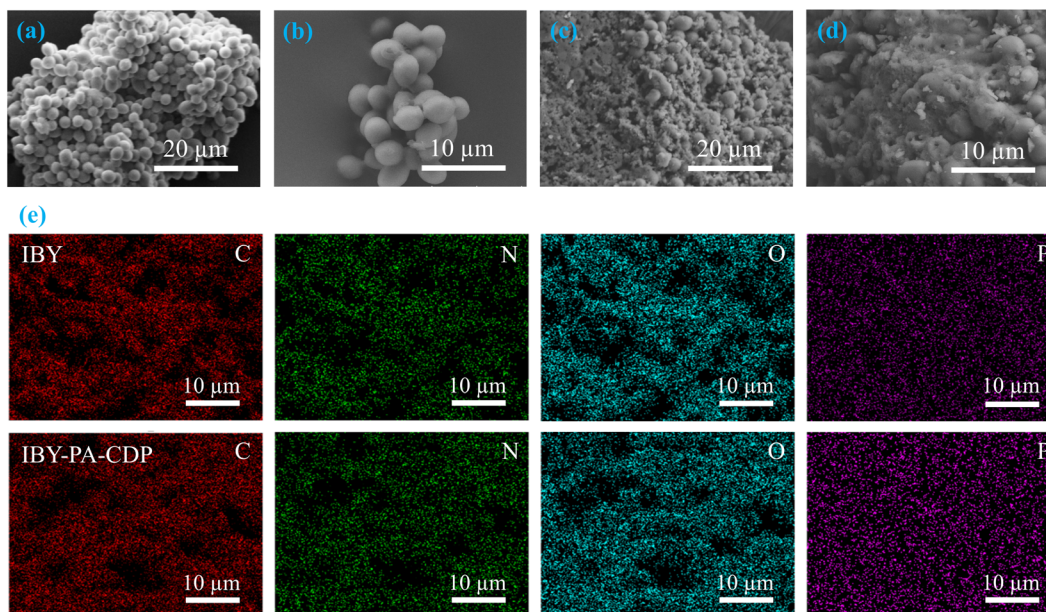
Fig. 2   SEM micrographs of (a and b) IBY, (c and d) IBY-PA-CDP; (e) elemental mapping of IBY, and IBY-PA-CDP.

5.66 mg g^{-1}. This is attributed to electrostatic interactions and other interactions that synergistically enhance the adsorption of MO by IBY-PA-CDP, such as van der Waals forces, hydrophobic interactions, hydrogen bonding, and host–guest interactions.[46] Interestingly, the MO adsorption capacity of IBY increased as the pH increased from 2 to 3. This may be because a more acidic solution altered the structure of the polymer on the IBY surface. The macroscopic changes of MB, BPA, and MO before and after adsorption are shown in Fig. S4,† and the color change of MB is particularly obvious.
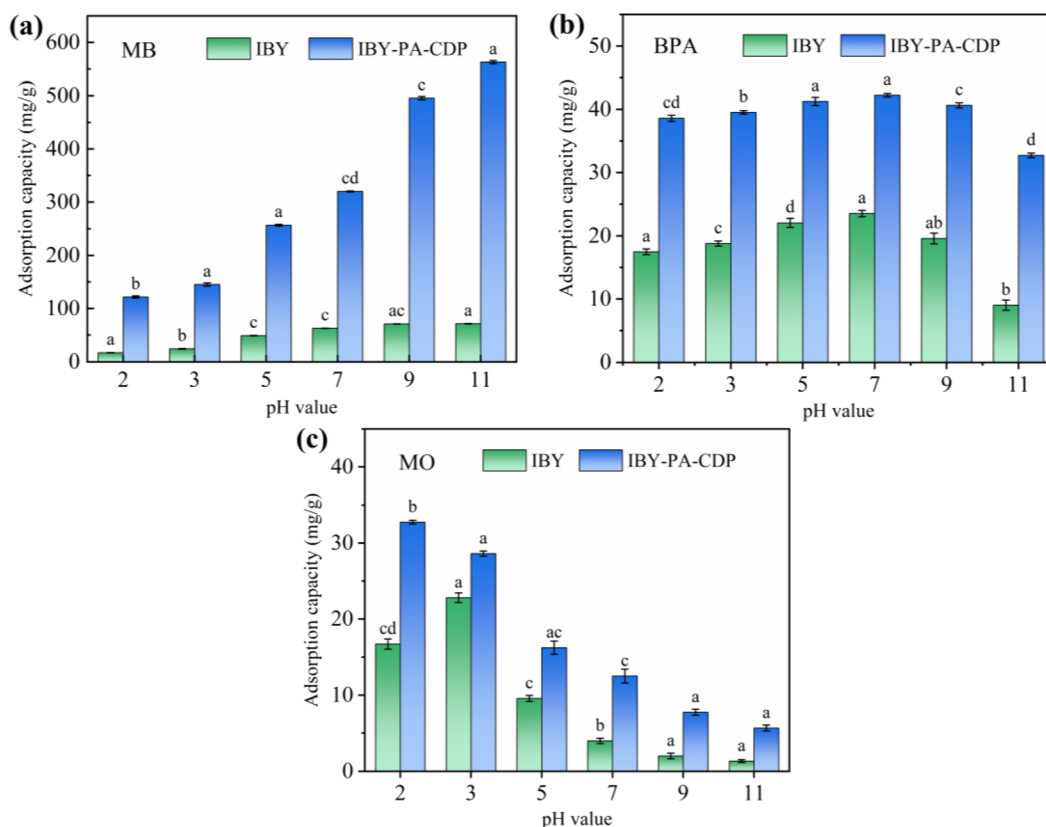

Fig. 3   Equilibrium adsorption capacity of IBY, and IBY-PA-CDP for (a) MB, (b) BPA, and (c) MO varying with pH.

3.2.2 Effects of temperature and IBY-PA-CDP dosage. Fig. 4a shows that the removal efficiencies of MB and BPA/MO exhibited opposite trends. The MB removal rate increased with increasing temperature (from 83.51% to 99.58%). First, MB strongly interacts with its active site. Second, an increase in temperature enhances the Brownian motion of the molecules in solution,[47] which increases the probability of collisions between the MB molecules and IBY-PA-CDP in solution. In contrast to MB, an increase in temperature led to a decrease in the removal of BPA and MO. This is because the bonding of BPA/MO to the active adsorbent sites is weaker at higher temperatures, particularly when physical interaction forces (hydrogen bonding and hydrophobic effect) are involved in adsorption.[48] Adsorption thermodynamics are investigated in the ESI† file of the manuscript. In conclusion, elevated temperatures favored MB adsorption by IBY-PA-CDP, but were detrimental to BPA/MO adsorption.

The effects of adsorbent dosage on MB/BPA/MO are shown in Fig. 4b. When the adsorbent dose was less than 1.0 g L^{-1}, MB/BPA/MO exhibited a higher adsorption capacity but a lower removal rate. Owing to the small amount of adsorbent, a portion of the target pollutant in the solution occupied almost all the active sites of the adsorbent, which caused the active sites to become saturated. However, a higher amount of the target contaminant was still present in the solution. When the dose of IBY-PA-CDP exceeded 1.0 g L^{-1}, the adsorbents provided more active adsorption sites to fully adsorb the target pollutants in the solution, thereby enhancing the removal rate. Furthermore, the dose of adsorbent added was greater than that required to remove the total amount of the target pollutant, which resulted in saturation of the active sites becoming difficult and decreasing the adsorption capacity.[49] Based on the cost of the adsorbent and removal rate of the modeled contaminants, the IBY-PA-CDP dose was set to 1.0 g L^{-1} in subsequent experiments.

3.2.3 Effect of contact time. Determining the response time of wastewater treatment is important for practical applications. As shown in Fig. 4c, a prolonged contact time evidently facilitated the adsorbent to fully adsorb the modeled pollutants. The IBY-PA-CDP adsorbent exhibited a rapid adsorption rate during the first 150 min. The target pollutant molecules move from solution to the surface of IBY-PA-CDP due to the concentration difference. Furthermore, adsorption begins with many adsorption sites for MB/BPA/MO, which provides a stronger driving force. However, over time, the number of free sites available for loading the modeled contaminants gradually decreased. Simultaneously, contaminants adsorbed at the active sites may block the channels, preventing residual vacancies from being
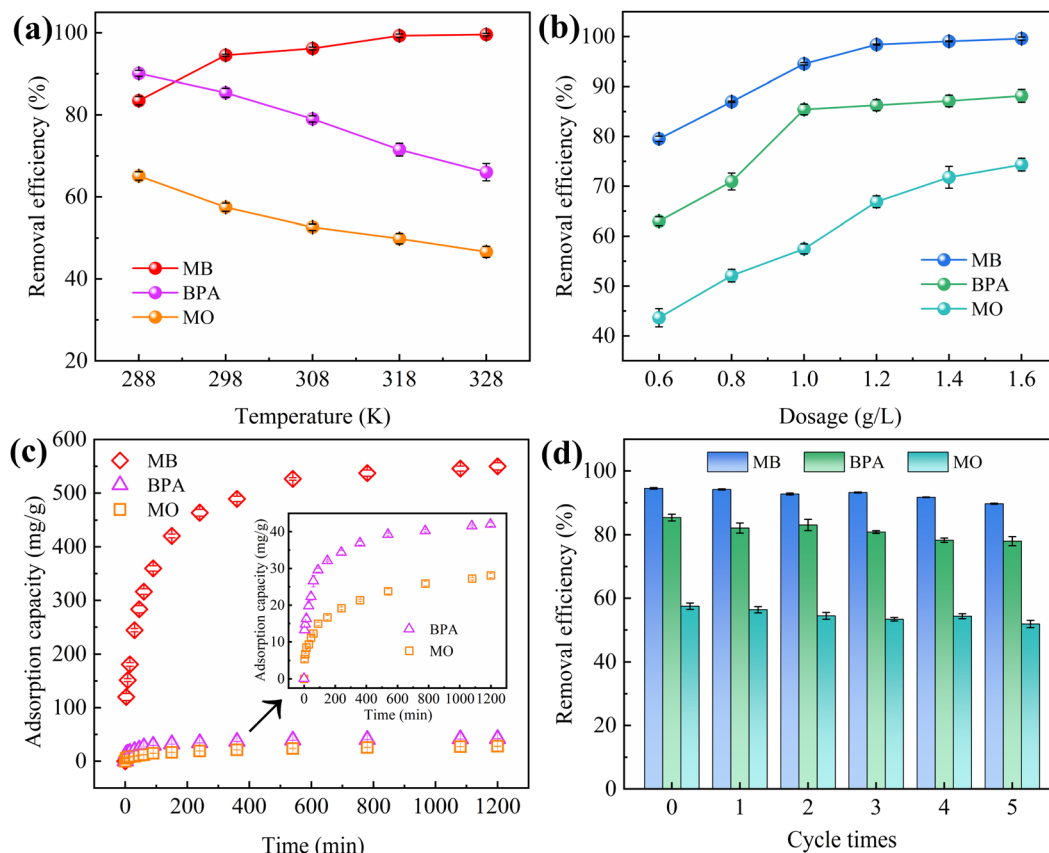

Fig. 4 (a) Influence of operating temperature on the removal efficiency of IBY-PA-CDP for MB, BPA, and MO; (b) influence of IBY-PA-CDP dosage on MB, BPA, and MO removal rate; (c) influence of contact time on the adsorption capacity of IBY-PA-CDP for MB, BPA, and MO; (d) influence of the number of regeneration cycles of IBY-PA-CDP on the removal rate for MB, BPA and MO.

occupied and slowing the adsorption rate until equilibrium is attained.[13] At high MB concentrations, the adsorption reached equilibrium after 780 min. The adsorption of lower concentrations of BPA and MO gradually reached equilibrium after 1080 min.

3.2.4 Reusability of IBY-PA-CDP. Recycling of adsorbents is important for assessing their application potential considering environment-friendliness and economic benefits. In this experiment, the same batch of adsorbent was used for the adsorption–desorption experiments, and the results of the regeneration performance of the adsorbent are shown in Fig. 4d. The removal efficiency of the adsorbent loaded with the modeled pollutants did not differ significantly after five regeneration cycles. The reduction in the removal performance of the materials was mainly due to the occupation of the reaction sites by the model pollutants caused by the high adsorption affinity of certain reaction sites for the model pollutants. This resulted in the incomplete desorption of the adsorbent. The results showed that IBY-PA-CDP can be effectively regenerated and reused with good stability and recyclability.

3.2.5 Effects of NaCl and humic acid. Ionic strength is one of the factors that affect the adsorption performance of adsorbents. NaCl, which is the most common salt in aqueous solutions, was used to study the effects of ionic strength. Fig. 5a shows that NaCl inhibits the adsorption of MB by IBY-PA-CDP and promotes the adsorption of BPA and MO. Both Na^+ and MB competitively bind to the oxygen-containing anionic groups through electrostatic interactions.[50] Therefore, with higher Na^+ concentration in the solution, more active sites were occupied. The addition of NaCl causes BPA to form molecules in multiple states. These molecules can penetrate deeper into the adsorbent surface. When hydrophobicity was the main driver of BPA adsorption, the presence of salt led to higher hydrophobicity of the associated surface and salt-induced dehydration.[51] These factors contribute to the adsorption of BPA to the reaction sites and improve the BPA removal efficiency. Furthermore, when hydrogen bonding is the main driving force for BPA adsorption by the adsorbent, an increase in salt concentration can lead to hydrogen bond salting out.[52] This made the adsorbent less capable of adsorbing BPA. The MO removal efficiency of anionic dyes was found to be substantially reduced with increasing ionic strength, confirming that electrostatic attraction is the primary mechanism of MO adsorption.[47] However, the results of the present study show a gradual increase in the MO removal efficiency by IBY-PA-CDP. This may be due to the dominant role of hydrophobic interactions in MO adsorption. This experiment also confirmed that the adsorbent material containing-CD adsorbed MO *via* hydrophobic interactions (host–guest interactions).

HA is a complex organic matter present in natural aquatic environments that usually coexists with dyes and endocrine disruptors, which may affect the adsorption performance of IBY-PA-CDP. Fig. 5b shows that as the initial concentration of HA increased, the removal of MB and MO decreased by 6.46% and 5.32%, respectively, and BPA showed a maximum removal decrease of 8.27%. HA is a macromolecule with many functional groups, including hydroxyl, aryl ring, carboxyl, and

carbonyl groups.[53] Therefore, HA may be bound to the surface of IBY-PA-CDP through hydrogen bonding and hydrophobic and electrostatic interactions, thus competing for active sites. MO was less strongly inhibited by HA than by MB. According to Wang *et al.*,[54] HA forms a spherical structure under acidic conditions, and this form of HA will occupy fewer active sites and reduce the spatial site resistance to favor its adsorption. The results showed that IBY-PA-CDP maintained good adsorption performance for removing MB, BPA, and MO, even in the presence of a large amount of HA.

3.2.6 Effects of strong acidic ionic salts. The results of the NaCl experiments described in Section 3.2.5 indicated that electrostatic interactions are not the primary mechanism by which IBY-PA-CDP adsorbs MO. To verify this result and further understand the mechanism of adsorption, experiments on the effect of the anions on MO were performed. As shown in Fig. 5c, the removal of MO by IBY-PA-CDP exhibits different degrees of elevation after adding the four salts. The anions in the salt solutions did not inhibit the adsorption of MO onto IBY-PA-CDP. This indicates a lack of competition between the anions and MO at the surface-active sites of IBY-PA-CDP. This also suggests that electrostatic interactions are not the main mechanism of MO adsorption by IBY-PA-CDP. The addition of $NaNO_3$ and Na_2SO_4 enhanced the removal of MO by 9.09% and 12.95%, respectively, compared to the control. The presence of Na^+ appeared to be responsible for this phenomenon. This suggests that hydrophobic interactions are the main drivers of adsorbed MO. Therefore, in combination with the experimental results described in Section 3.2.1, the mechanism of MO adsorption by IBY-PA-CDP involves electrostatic and hydrophobic interactions. Among the four salts, NaH_2PO_4 was the most effective at promoting MO adsorption by IBY-PA-CDP. The presence of sodium ions increased the hydrophobicity. Moreover, the ionization of hydrogen ions in dihydrogen phosphate lowered the pH of the water after NaH_2PO_4 was added to the aqueous solution.

3.2.7 Effect of metal ions. In addition to alkaline conditions, acidic solutions favored MB adsorption by IBY-PA-CDP (Section 3.2.1). Natural and industrial wastewater contain various metal cations that may inhibit MB removal. Therefore, the influence of light and heavy metal ions on the adsorption of MB by IBY-PA-CDP was investigated at pH 4 (Fig. 5d). The MB removal efficiency in solutions containing divalent metal cations (Ca^{2+}, Co^{2+}, Mn^{2+}, and Cu^{2+}) decreased more considerably than in those containing monovalent metal cations (K^+). This indicated that the higher the charge number of the metal ions, the stronger their electrostatic interactions with the carboxyl and phosphate groups of IBY-PA-CDP,[55] which inhibited the removal of MB by IBY-PA-CDP to a greater extent. Among these metal ions, Cu^{2+} had the greatest inhibitory effect on MB adsorption by IBY-PA-CDP, resulting in a decrease in MB removal efficiency from 99.54% to 85.15%. This is because of the larger hydrated ionic radius and the electron-shielding effect of Cu^{2+}.[56,57] The spatial site resistance effect is a common mechanism affecting adsorption performance during adsorption. In general, the larger the hydrated ionic radius of an ion and the more pronounced the spatial site barrier effect, the greater its ability to hinder the adsorption of cationic substances.[58] Among the divalent metal cations, the hydration
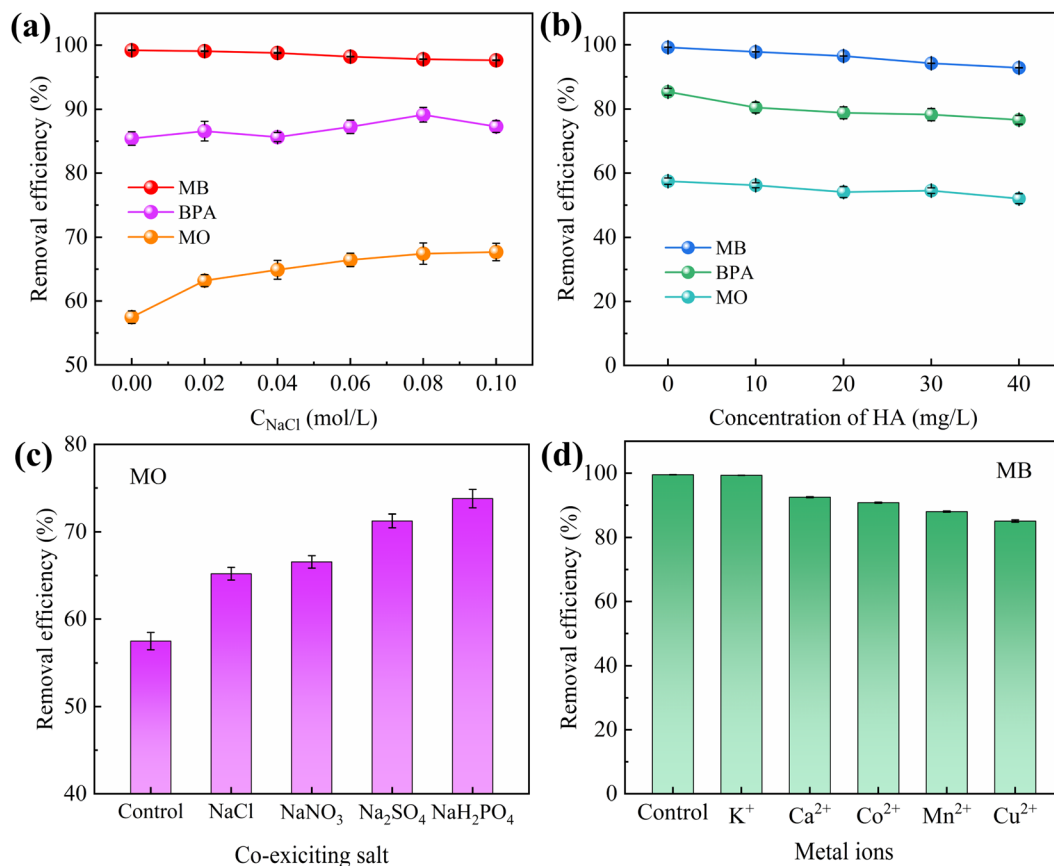
Fig. 5 Effects of (a) ionic strength and (b) HA on removal efficiency of MB, BPA, and MO using IBY-PA-CDP; (c) effects of strong/weak acid ionic salts on the adsorption of MO by IBY-PA-CDP; (d) effect of metal ions on removal efficiency of IBY-PA-CDP for MB.

radius of Cu^{2+} (4.19 Å) > Ca^{2+} (4.12 Å). This is consistent with the result that Cu^{2+} inhibits the adsorption of MB more than Ca^{2+}. The results showed that IBY-PA-CDP exhibited excellent MB adsorption performance in metal ion solutions.

3.3 Removal of pollutants from binary mixture by the IBY-PA-CDP

Although IBY-PA-CDP can effectively adsorb a single target pollutant, its adsorption performance for each pollutant in a binary organic pollutant system remains unclear. Fig. 6a and c–e show that the removal rates of BPA and MO in the binary system were still characterized by the pH response, and the trends were the same as those in the single system. The BPA removal efficiency decreased in the presence of MB/MO (Fig. 6a and c). This is because BPA, MB, and MO can be stably contained in the cavity of β-CD through host-guest interactions.[59–61] Hydrophobic interactions also promote the adsorption of both BPA and MO by IBY-PA-CDP (Section 3.2.5). Moreover, IBY-PA-CDP adsorbed MB faster than BPA (Section 3.2.3). Therefore, IBY-PA-CDP preferentially adsorbed MB in a mixed solution of BPA + MB. The large amount of MB adsorbed on the surface of IBY-PA-CDP may increase the spatial site resistance to intra-particle diffusion, thereby hindering the adsorption of BPA to the active sites.[54] Similarly, the spatial site resistance and competition for the same active site led to a decrease in the

removal of MO in the BPA + MO binary system (Fig. 6d). However, very high MB removal efficiencies (Fig. 6b and f) were achieved despite the change in solution pH and the addition of BPA/MO. This indicates that MB was not affected by the presence of BPA/MO. This was due to the high adsorption of MB by the adsorbent, which completely removed low concentrations of MB from the mixed solution.

In the BPA/MO and BPA/MB binary systems, the removal rate of BPA/MO decreased when another modeled pollutant was added. However, substantial amounts of MO were adsorbed when MO and MB co-existed (Fig. 6e). That is, MB promoted IBY-PA-CDP adsorption by MO. A plausible explanation for this is that the MB molecules adsorbed on the surface of IBY-PA-CDP act as bridges (Fig. 7). The specific mechanisms are as follows: due to the aromatic ring structure of MB, two MB molecules can form stacked, head-to-tail adjacent dimers in solution by π–π stacking.[62] The protonated tertiary amino group of one MB molecule in the MB dimer was attracted by the deprotonated carboxyl and phosphate groups of IBY-PA-CDP, whereas the protonated tertiary amino group of the other MB molecule attracted MO with a sulfonic acid group.[63] Therefore, the MO removal rate of IBY-PA-CDP was higher in the MO + MB dimer system. Compared to the acidic system (pH 2–7), the alkaline system (pH 7–11) better promoted the adsorption of MO. The more alkaline the solution, the more negatively charged the IBY-
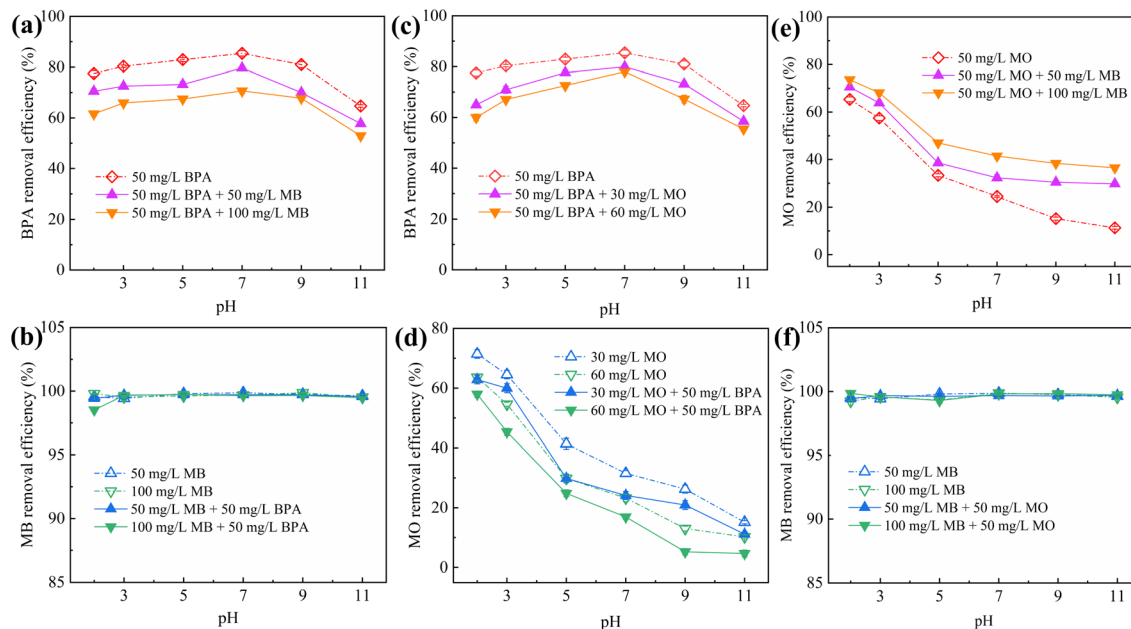
Fig. 6 Effect of pH on the adsorption of BPA (a and c), MB (b and f) and MO (d and e) by IBY-PA-CDP in binary systems.

PA-CDP and the greater the drive to adsorb MB. This strong driving force quickly pulled all the MB molecules into the solution, and the fast-moving MB molecules carried more MO molecules to the adsorbent surface.

In summary, MB, BPA, and MO could be adsorbed onto IBY-PA-CDP in a mixed solution. Moreover, the addition of BPA hindered the adsorption of MO. The presence of BPA/MO did not considerably affect MB adsorption. However, the presence of MB can improve the removal efficiency of MO by the adsorbent owing to the bridging effect.

3.4 Adsorption kinetics

Plots of the curves and associated parameters fitted using the kinetic data and model are in Fig. 8a–c and Table S3.† The correlation coefficients R^2 (0.986–0.944) of the Elovich model are higher than those of the PFO (0.862–0.906) and PSO (0.930–0.961). This suggests that the removal of MB, BPA, and MO by IBY-PA-CDP is a chemical process occurring on nonhomogeneous surfaces.[64] The fitting of the Elovich model to the experimental data yielded the following values for the three target pollutants: MB (51.054), BPA (9.303), and MO (1.233). Compared with BPA
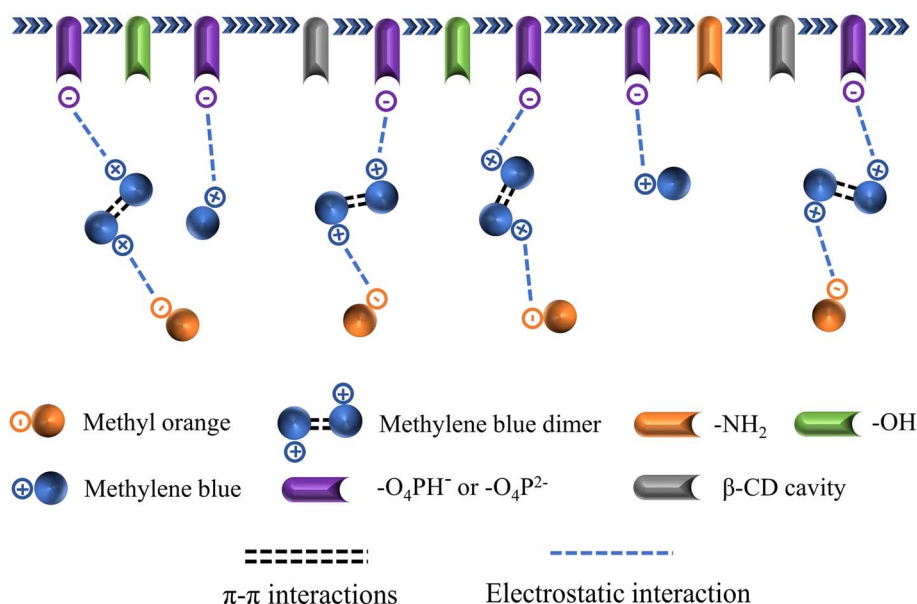

Fig. 7 Proposed mechanism of MB enhancement of IBY-PA-CDP adsorption of MO.

and MO, IBY-PA-CDP was superior for MB adsorption. The presence of more effective MB-binding sites on the adsorbent surface resulted in a stronger driving force for MB with IBY-PA-CDP.

3.5 Adsorption isotherms

The fitted curves and parameters of the three isothermal models are shown in Fig. 8d–f and Table S4.† For MB and BPA, the Langmuir model had the best fit among the three models ($R^2 = 0.992, 0.941$), indicating that the adsorption process for MB and BPA was mainly homogeneous monolayer adsorption. The calculated R_L values for MB and BPA ranged between 0.0015–0.0056 and 0.0714–0.2778, respectively, indicating that the Langmuir isotherm was highly favorable under the experimental conditions studied. For MO, the Freundlich isotherm model revealed a higher correlation coefficient value ($R^2 = 0.990$) closer to 1, suggesting that MO adsorption on IBY-PA-CDP is a non-homogeneous multilayered adsorption process and that the energy of biosorption decreases exponentially as the adsorption sites on the adsorbent become saturated.[65] Meanwhile, the parameter $1/n = 0.52$ confirms the advantage of this model in fitting the adsorption of MO.[66]

3.6 Mass transfer mechanisms

A mass transfer mechanism model was used to explore the mechanisms and rate-limiting steps in the adsorption of target pollutants by the adsorbents. The uptake of the adsorbate in solution by the adsorbent is essentially a mass-transfer process, that is, the adsorbent is transferred from the solution to the surface of the adsorbent and bound to the adsorption site by physical or chemical forces. This process consists of three main stages. External diffusion: transfer of MB/BPA/MO from the solution to the interior of the liquid film on the surface of IBY-PA-CDP; internal diffusion: transfer of MB/BPA/MO in the internal pores of IBY-PA-CDP upon reaching the interior of the liquid film and adsorption of MB/BPA/MO in the pores to the active sites of IBY-PA-CDP.[67]

3.6.1 External diffusion model. The external diffusion (EXD) model assumes that external diffusion is the slowest stage of mass transfer. The Mathews and Weber model was used as the EXD model to explain the movement of the dye/bisphenol molecules in solution to diffuse into the IBY-PA-CDP boundary layer.[68] The difference in the concentration between the adsorbate inside and outside the liquid membrane was the driving force. The model assumes that the adsorbate diffusion in the boundary liquid film around the adsorbent is the main rate-limiting step. The external diffusion process is expressed as:

$$k_{\mathrm{MW}} = \frac{r_0 \rho (1 - \varepsilon)}{3 m_{\mathrm{s}}} \frac{\ln(C_0/C_t)}{t} \tag{1}$$

where k_{MW} denotes the mass transfer coefficient (cm min^{-1}), and the coefficient term $\frac{3 m_{\mathrm{s}}}{r_0 \rho (1 - \varepsilon)}$ can be replaced by the external surface coefficient S (cm^{-1}). Rearranging eqn (1) yields

$$\frac{C_t}{C_0} = \mathrm{e}^{-k_{\mathrm{MW}} S t} \tag{2}$$

where the value of $k_{\mathrm{MW}} S$ is used to characterize the external diffusion.

$$q_t = \frac{V}{m}(C_0 - C_t) = \frac{C_0 - C_t}{m_{\mathrm{v}}} \tag{3}$$

where m_{v} is the mass of the adsorbent per unit volume of the solution (g L^{-1}).
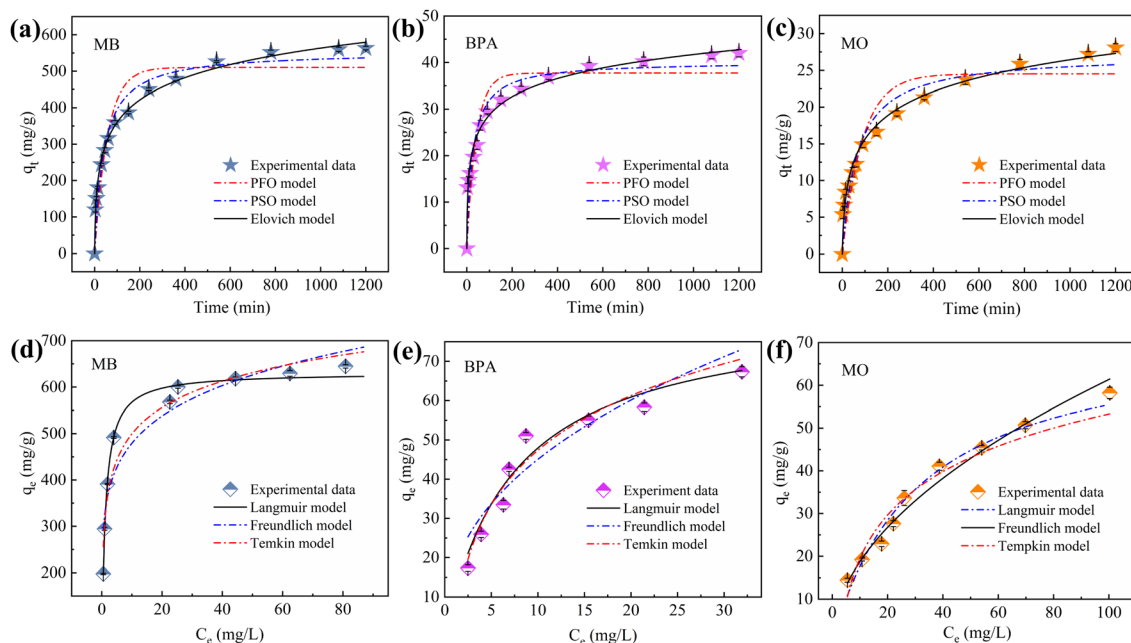

Fig. 8 Fitting curves for kinetics of MB (a), BPA (b) and MO (c) adsorbed by IBY-PA-CDP. Fitting curves of MB (d), BPA (e) and MO (f) on IBY-PA-CDP obtained from Langmuir, Freundlich, and Tempkin models.

Paper

This is obtained by combining eqn (2) and (3):

$$q_t = \frac{C_0}{m_v}\left(1 - e^{-k_{MW}St}\right) \tag{4}$$

3.6.2 Internal diffusion model. The internal diffusion (IND) model considers internal diffusion as the slowest stage of mass transfer, which can be expressed using a modified intra-particle diffusion model.[69] The intra-particle diffusion model used by many researchers is as follows:

$$q_t = k_i t^{0.5} + C \tag{5}$$

where k_i [mg $(g^{-1}\ min^{-0.5})$] is the intra-particle diffusion rate coefficient and C (mg g^{-1}) is the constant term of the linear fit.

In the actual experiment, the absorption reaction did not begin at $t = 0$. Therefore, $q_{t=0} = 0$, $C = 0$. However, the C value obtained by most researchers using eqn (5) was not zero. This is not consistent with observed results. Thus, a point ($t = 0$, $q_{t=0} = 0$) is required as an initial condition for the IND model.

In the present study, a new model of intra-particle diffusion is proposed. We assumed that the adsorbate in the solution diffuses into the pores at the beginning of the experiment, and then diffusion within the pores reaches equilibrium at t_1, which is the first stage of the internal diffusion model (IND model-1). This is represented by a curve through (0, 0) at time $t \in [0, t_1]$:

$$q_t = k_1 t^{0.5} \tag{6}$$

After time t_1, the adsorbate in the pores binds to the active site, the equilibrium of internal diffusion in the pores is broken, and the adsorbate in the solution diffuses into the pores until it binds to the active sites. This was the second stage of internal diffusion (IND model-2). For time $t \in [t_1, t_2]$, IND model-2 is described as follows:

$$q_t - q_{t_1} = k_2(t - t_1)^{0.5} \tag{7}$$

In summary, the modified form of the intra-particle diffusion model is:

$$q_t = k_1 t^{0.5},\ 0 \le t \le t_1 \tag{8}$$

$$q_t - q_{t_1} = k_2(t - t_1)^{0.5},\ t_1 < t \le t_2 \tag{9}$$

where k_1 [mg $(g\ min)^{-0.5}$] and k_2 [mg $(g\ min)^{-0.5}$] are the rate constants of intra-particle diffusion.

3.6.3 Adsorption on active site model. In this section, we use the Ritchie's equation as an active site adsorption model (ADAS model).[64] Ritchie's equation assumes that adsorption on the active site is the slowest stage in the mass transfer process, suggesting that an adsorbate can bind to n active adsorption sites. The Ritchie's equation is expressed in eqn (10):[70]

$$\frac{d\theta}{dt} = \alpha(1 - \theta)^n \tag{10}$$

where θ ($0 \le \theta \le 1$) is denoted as the occupied active site ratio. After integrating for the initial conditions $t = 0$ and $\theta = 0$, Ritchie's equation becomes:

For $n = 1$,

$$\theta = 1 - e^{-\alpha t} \tag{11}$$

For $n \ne 1$,

$$\theta = 1 - [1 + (n - 1)\alpha t]^{1/1-n} \tag{12}$$

where θ can be described by the ratio of q_t to q_m (q_m can be obtained from the Langmuir isotherm model), eqn (11) and (12) become.

For $n = 1$,

$$q_t = q_m(1 - e^{-\alpha t}) \tag{13}$$

For $n \ne 1$,

$$q_t = q_m - q_m[1 + (n - 1)\alpha t]^{1/1-n} \tag{14}$$

where α is the rate constant (min^{-1}) and eqn (13) is the same as that in the pseudo-first-order kinetic model (S4). Therefore, eqn (14) was used as the ADAS model for adsorption fitting.

The Freundlich isotherm model did not yield the maximum adsorption capacity q_m. Therefore, the ADAS model cannot be fitted using an experimental model. The mass transfer kinetics were fitted to the experimental data for MB and BPA using the EXD, IND, and ADAS models. Fig. 9 shows the plots of the fitted mass-transfer kinetic models, and Table S5† summarizes the calculated parameters for each model. Among the three mass-transfer kinetic models, the ADAS model exhibited the highest correlation coefficients for the kinetic data fitted to MB and BPA. These results indicate that adsorption on the active sites was the main rate-limiting step in the mass transfer of MB and BPA. Since IBY-PA-CDP contains numerous phosphate groups and β-cyclodextrin cavities. Therefore, a longer time was required to saturate the active adsorption sites. These results also illustrate that the external and internal diffusion of MB and BPA into IBY-PA-CDP is rapid. The hydrophilicity and hydrophobicity of IBY-PA-CDP led to the rapid passage of MB and BPA molecules through the liquid membrane between IBY-PA-CDP and the aqueous solution, respectively (i.e., rapid external diffusion). The small specific surface area allows the MB and BPA molecules to quickly reach the active adsorption sites through an intra-particle path (i.e., rapid internal diffusion). Moreover, the electrostatic, hydrophobic, and host–guest interactions between IBY-PA-CDP, MB, and BPA effectively increased the diffusion rates of MB and BPA in the liquid membrane and pores. Therefore, the rate-limiting step must be investigated to better understand the mechanism of adsorption onto the adsorbent.

3.7 Proposed sorption mechanism

To further explore the possible interactions between MB/BPA/MO and IBY-PA-CDP, the high-resolution XPS and FTIR spectra before and after adsorption were analyzed (Fig. 10 and S1†).

Hydrogen bonding is one of the most common mechanisms involved in the adsorption of organic pollutants. Fig. S1† shows that after MB and MO were adsorbed by IBY-PA-CDP, the peaks
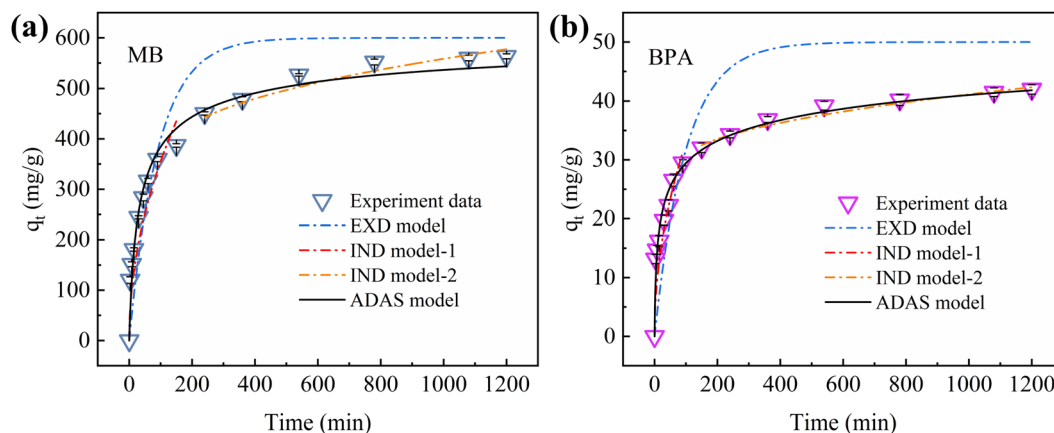
Fig. 9 Experimental data fitting for MB (a) and BPA (b) adsorption on IBY-PA-CDP by EXD, IND, and ADAS models.

shifted to 3413 and 3418 cm^{-1} at 3424 cm^{-1}, respectively, suggesting that –OH is involved in the formation of hydrogen bonds.[71] The disappearance of the –OH bending vibrational peak of PA at 1704 cm^{-1} in IBY-PA-CDP/BPA indicated that the hydroxyl group on BPA was hydrogen-bonded to IBY-PA-CDP. As shown in Fig. 10a–d, when MB, BPA, and MO were adsorbed, the peak at C–OH shifted from 284.93 eV to 285.45 eV, 285.31 eV, and 285.42 eV, respectively, which suggests that hydroxyl groups on the adsorbent were involved in adsorption of the modeled pollutants. C–OH can act as a hydrogen donor to
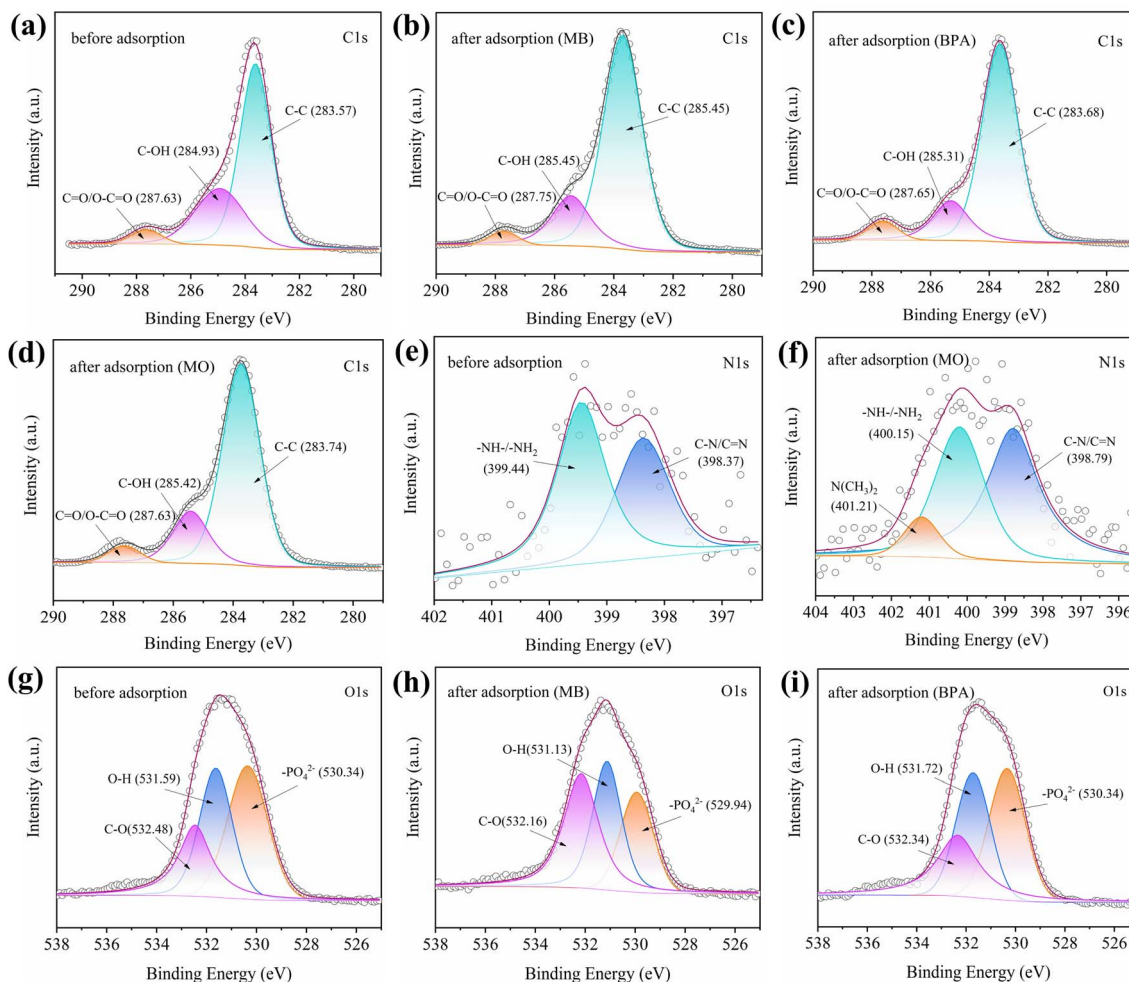

Fig. 10 Spectra of (a–d) C 1s, (e and f) N 1s and (g–i) O 1s for IBY-PA-CDP before and after of adsorption MB, BPA, and MO.

form hydrogen bonds.[72] A deconvoluted peak corresponding to O–H was observed in the O 1s spectrum at 531.59 eV (Fig. 10g). When MB and BPA are adsorbed, the peaks at O–H are shifted to 531.13 eV and 537.72 eV, respectively, which is attributed to the oxygen atoms in the O–H that act as hydrogen acceptors to provide lone electron pairs for hydrogen-bonding interactions with MB and BPA.

Electrostatic interactions are considered important mechanisms for dye adsorption. As presented in Fig. S1,† for IBY-PA-CDP/MO, the peak at 1632 cm^{-1} shifted to 1627 cm^{-1}, suggesting that the N–H groups in the adsorbent can be used to adsorb MO.[50] The protonated amino group of IBY-PA-CDP can be assumed to be involved in electrostatic interactions with the sulfonic acid group of MO. The disappearance of the peak near 1704 cm^{-1} for IBY-PA-CDP/MB indicated that the phosphate group was used to adsorb MB. We observed a deviation of 0.12 eV in the binding energy of IBY-PA-CDP/MB at C=O/O–C=O compared to the original binding energy (Fig. 10a and b), which might have been caused by the electrostatic interaction between MB and the carboxyl group. As shown in Fig. 5 and 6e, after the adsorption of MO, a new characteristic peak at 401.21 eV in the N 1s spectrum correlates with the $N(CH_3)_2$ of MO.[73] Meanwhile, the peak of IBY-PA-CDP/MO at 399.44 eV of the N 1s spectrum is shifted to 400.15 eV, which implies that –NH–/–NH_2 is involved in the electrostatic interaction. For O 1s, the peak at 530.34 eV is attributed to the –PO_4^{2-} group of phytate (Fig. 10g). After MB adsorption, the peak at –PO_4^{2-} becomes 529.94 eV, which may be attributed to the electrostatic attraction between the negatively charged oxygen group (–PO_4^{2-}) of IBY-PA-CDP and the positively charged nitrogen atoms of dimethylimine (=N^+Me_2) on MB.[74]

However, considering the presence of the hydrophobic cavity of β-CD, IBY-PA-CDP may effectively adsorb hydrophobic pollutants through strong hydrophobic interactions. Ionic strength studies suggested that hydrophobic interactions may be the main driving force for the adsorption of BPA and MO (Section 3.2.5). A study of strongly acidic ionic salts further verified that the main factor for MO adsorption by IBY-PA-CDP was the hydrophobic interactions (Section 3.2.6).

Finally, MB, BPA, and MO have linear structures that match the cavity of β-CD.[60] The β-CD cavity was found to contain part of the structure of MB/MO molecules, or multiple β-CD molecules can form a network structure to capture dye molecules.[25] However, the β-CD cavity forms a stable inclusion complex with BPA.[26] As shown in Fig. S1,† the change in the displacement of the –OH bending vibration from 1632 cm^{-1} to 1609, 1623, and 1627 cm^{-1} may be a result of the inclusion of MB/BPA/MO into the-CD cavity. Therefore, MB, BPA, and MO can be inferred to be adsorbed by IBY-PA-CDP as "guests" through host–guest interactions.

4. Conclusion

In this study, Baker's yeast, β-CD, and phytic acid were used to synthesize insoluble and multifunctional biomass polymer (IBY-PA-CDP) composites *via* a simple cross-linking reaction and this composite was used to treat MB, BPA, and MO in aqueous solutions. This study showed that MB, BPA, and MO could be adsorbed onto IBY-PA-CDP in single and binary systems solutions. The addition of humic acid and metal ions decreased the adsorption capacity of IBY-PA-CDP for MB owing to competitive adsorption. Adsorption studies on model pollutant binary systems showed that MB/MO inhibited the adsorption of BPA by IBY-PA-CDP. In contrast, the presence of MB enhanced the removal rate of MO by IBY-PA-CDP owing to the bridging effect. The adsorption models demonstrated that the adsorption of MB/BPA by IBY-PA-CDP was dominated by monolayer chemisorption, and that the adsorption of MO was multilayer chemisorption. Electrostatic interactions were the main driving force of MB adsorption by IBY-PA-CDP. Hydrophobic interactions were the main factors leading to the adsorption of BPA and MO. In addition, the β-CD cavity contained in IBY-PA-CDP can trap MB/BPA/MO based on the host-guest interactions. The present study analyzed and investigated the adsorption behavior and mechanism of three organic pollutants with different electrical properties. The synthesized Baker's yeast–cyclodextrin polymer composites can potentially be employed to treat wastewater containing MB, BPA, and MO.

Author contributions

Zhikun Lv: investigation, conceptualization, writing of the original draft, formal analysis and methodology. Zhaoyang Wang & Huaiguang Wang: data curation, investigation and formal analysis, conceptualization, methodology. Jianbin Li & Kai Li: supervision, funding acquisition, and project administration.

Conflicts of interest

The authors declare that they have no known competing financial interests or personal relationships that could have appeared to influence the work reported in this paper.

Acknowledgements

References

1 F. T. Geldasa, M. A. Kebede, M. W. Shura and F. G. Hone, *RSC Adv.*, 2023, **13**, 18404–18442.

2 M. I. Khan, T. K. Min, K. Azizli, S. Sufian, H. Ullah and Z. Man, *RSC Adv.*, 2015, **5**, 61410–61420.

3 D. Bhatia, N. R. Sharma, J. Singh and R. S. Kanwar, *Crit. Rev. Environ. Sci. Technol.*, 2017, **47**, 1836–1876.

4 M. D. Khan, D. Li, S. Tabraiz, B. Shamurad, K. Scott, M. Z. Khan and E. H. Yu, *Sci. Total Environ.*, 2021, **756**, 143752.

5 J. Xiao, W. Lv, Z. Xie, Y. Tan, Y. Song and Q. Zheng, *J. Mater. Chem. A*, 2016, **4**, 12126–12135.

6 C. Lei, F. Wen, J. Chen, W. Chen, Y. Huang and B. Wang, *Polymer*, 2021, **213**, 123316.

7 Z. Zhou, Q. Guo, Z. Xu, L. Wang and K. Cui, *Environ. Eng. Sci.*, 2015, **32**, 203–211.

8 A. Kanwal, R. Rehman, M. Imran, G. Samin, M. M. Jahangir and S. Ali, *RSC Adv.*, 2023, **13**, 26455–26474.

9 N. A. H. Ismail, S. Y. Wee, N. H. Kamarulzaman and A. Z. Aris, *Environ. Pollut.*, 2019, **249**, 1019–1028.

10 D. Aksu Demirezen, D. Demirezen Yılmaz and Y. Ş. Yıldız, *Int. J. Biol. Macromol.*, 2023, **239**, 124311.

11 Z. M. Lazim, T. Hadibarata, M. H. Puteh and Z. Yusop, *Water, Air, Soil Pollut.*, 2015, **226**, 34.

12 M. El Khomri, N. El Messaoudi, A. Dbik, S. Bentahar, Y. Fernine, A. Lacherai and A. Jada, *Chem. Afr.*, 2022, **5**, 1083–1095.

13 E. Y. S. Soh, S. S. Lim, K. W. Chew, X. W. Phuang, V. M. V. Ho, K. Y. H. Chu, R. R. Wong, L. Y. Lee and T. J. Tiong, *Environ. Res.*, 2022, **204**, 112385.

14 K. Grace Pavithra, P. Sundarrajan, J. Arun, K. Brindhadevi, Q. Hoang Le and A. Pugazhendhi, *Environ. Res.*, 2023, 117005, DOI: 10.1016/j.envres.2023.117005.

15 Y. Wu, Y. Hu, Z. Xie, S. Feng, B. Li and X. Mi, *Appl. Biochem. Biotechnol.*, 2011, **163**, 882–894.

16 P. Saravanan, S. Kumaran, S. Bharathi, P. Sivakumar, P. Sivakumar, S. R. Pugazhvendan, W. Aruni and S. Renganathan, *Environ. Technol. Innovation*, 2021, **22**, 101442.

17 I. Shahzadi, Y. Wu, H. Lin, J. Huang, Z. Zhao, C. Chen, X. Shi and H. Deng, *J. Hazard. Mater.*, 2023, **453**, 131312.

18 Z. Duan, M. Song, T. Li, S. Liu, X. Xu, R. Qin, C. He, Y. Wang, L. Xu and M. Zhang, *RSC Adv.*, 2018, **8**, 31542–31554.

19 S. Liu, Z. Duan, C. He, X. Xu, T. Li, Y. Li, X. Li, Y. Wang and L. Xu, *RSC Adv.*, 2018, **8**, 8026–8038.

20 M. A. E. Bakhite, N. J. Sithole, L. S. Magwaza, A. O. Odindo, S. T. Magwaza and K. Ncama, *Heliyon*, 2021, **7**, e07912.

21 H. You, J. Chen, C. Yang and L. Xu, *Colloids Surf., A*, 2016, **509**, 91–98.

22 K. Bouaouina, A. Barras, N. Bezzi, M. A. Amin, S. Szunerits and R. Boukherroub, *Chemosphere*, 2022, **297**, 134188.

23 G. Crini, *Chem. Rev.*, 2014, **114**, 10940–10975.

24 Y.-L. Hong, J. Sun, X.-Q. Fang, Q.-W. Liu, C. Wang and C.-M. Liu, *Carbohydr. Polym.*, 2023, **316**, 121059.

25 J. Lagiewka, A. Nowik-Zajac, A. Pajdak and I. Zawierucha, *Carbohydr. Polym.*, 2023, **307**, 120615.

26 Z. Li, C. Hu, Z. Hu, Y. Fu and Z. Chen, *Carbohydr. Polym.*, 2022, **276**, 118786.

27 K. Zhou, Y. Li, Q. Li, Q. Du, D. Wang, K. Sui, C. Wang, H. Li and Y. Xia, *J. Polym. Environ.*, 2018, **26**, 3362–3370.

28 A. Alsbaiee, B. J. Smith, L. Xiao, Y. Ling, D. E. Helbling and W. R. Dichtel, *Nature*, 2016, **529**, 190–194.

29 J.-w. Wang, D. Lan, L. Yong-qiang, R.-f. Li, X.-t. Yang, G.-h. Lan, H.-y. Qiu and B. Xu, *Carbohydr. Res.*, 2021, **501**, 108276.

30 Q. Liu, Y. Zhou, J. Lu and Y. Zhou, *Chemosphere*, 2020, **241**, 125043.

31 F. M. Mpatani, A. A. Aryee, A. N. Kani, Q. Guo, E. Dovi, L. Qu, Z. Li and R. Han, *Chemosphere*, 2020, **259**, 127439.

32 S. Tonk and E. Rápó, *Int. J. Mol. Sci.*, 2022, **23**, 126334.

33 Y. Xia, L. Meng, Y. Jiang, Y. Zhang, X. Dai and M. Zhao, *Chem. Eng. J.*, 2015, **259**, 927–935.

34 A. Mora-Boza, M. L. López-Donaire, L. Saldaña, N. Vilaboa, B. Vázquez-Lasa and J. San Román, *Sci. Rep.*, 2019, **9**, 11491.

35 K.-H. Sun, Z. Liu, C. Liu, T. Yu, T. Shang, C. Huang, M. Zhou, C. Liu, F. Ran, Y. Li, Y. Shi and L. Pan, *Sci. Rep.*, 2016, **6**, 23931.

36 L. Wang, X. Zhu, X. Chen, Y. Zhang, H. Yang, Q. Li and J. Jiang, *Ind. Crops Prod.*, 2022, **182**, 114921.

37 K. Hemine, N. Łukasik, M. Gazda and I. Nowak, *J. Hazard. Mater.*, 2021, **418**, 126286.

38 P. Awasthi, R. S. Bangari and N. Sinha, *J. Mol. Liq.*, 2023, **370**, 120970.

39 J. C. Serrano-Niño, A. Cavazos-Garduño, F. Cantú-Cornelio, A. F. González-Córdova, B. Vallejo-Córdoba, A. Hernández-Mendoza and H. S. García, *LWT–Food Sci. Technol.*, 2015, **64**, 1334–1341.

40 A. Sánchez-Iglesias, M. Grzelczak, T. Altantzis, B. Goris, J. Pérez-Juste, S. Bals, G. Van Tendeloo, S. H. Donaldson Jr, B. F. Chmelka, J. N. Israelachvili and L. M. Liz-Marzán, *ACS Nano*, 2012, **6**, 11059–11065.

41 N. S. Tezerji, M. M. Foroughi, R. R. Bezenjani, N. Jandaghi, E. Rezaeipour and F. Rezvani, *Food Chem.*, 2020, **311**, 125747.

42 M. J. Puchana-Rosero, E. C. Lima, S. Ortiz-Monsalve, B. Mella, D. da Costa, E. Poll and M. Gutterres, *Environ. Sci. Pollut. Res.*, 2017, **24**, 4200–4209.

43 H. A. Said, I. Ait Bourhim, A. Ouarga, I. Iraola-Arregui, M. Lahcini, A. Barroug, H. Noukrati and H. Ben youcef, *Int. J. Biol. Macromol.*, 2023, **225**, 1107–1118.

44 M. Xiao, F. Yang, S. Im, D. S. Dlamini, D. Jassby, S. Mahendra, R. Honda and E. M. V. Hoek, *J. Membr. Sci. Lett.*, 2022, **2**, 100022.

45 L. Xu, T. Bai, X. Yi, K. Zhao, W. Shi, F. Dai, J. Wei, J. Wang and C. Shi, *Int. J. Biol. Macromol.*, 2023, **238**, 124131.

46 N. Du, L.-Y. Huang, Y.-S. Xiong, R. Tian, J.-Y. Yin, D.-Y. Cao, D.-B. Hu, H.-Q. Lu, W. Li and K. Li, *Carbohydr. Polym.*, 2023, **313**, 120855.

47 S.-z. Hu, T. Huang, N. Zhang, Y.-z. Lei and Y. Wang, *Sep. Purif. Technol.*, 2022, **297**, 121470.

48 N. Tahari, P. L. de Hoyos-Martinez, N. Izaguirre, N. Houwaida, M. Abderrabba, S. Ayadi and J. Labidi, *Int. J. Biol. Macromol.*, 2022, **210**, 94–106.

49 M. K. Uddin and U. Baig, *J. Cleaner Prod.*, 2019, **211**, 1141–1153.

50 K. Li, X. Li and B. Li, *Sep. Purif. Technol.*, 2022, **289**, 120737.

51 G. Xu, X. Xie, L. Qin, X. Hu, D. Zhang, J. Xu, D. Li, X. Ji, Y. Huang, Y. Tu, L. Jiang and D. Wei, *Green Chem.*, 2019, **21**, 6062–6072.

52 H. Ding, Z. Zhang, Y. Li, L. Ding, D. Sun and Z. Dong, *Bioresour. Technol.*, 2022, **364**, 128018.

53 X. Hu, G. Xu, H. Zhang, M. Li, Y. Tu, X. Xie, Y. Zhu, L. Jiang, X. Zhu, X. Ji, Y. Li and A. Li, *ACS Appl. Mater. Interfaces*, 2020, **12**, 12165–12175.

54 J. Wang, C. Wang, A. Shi, Y. Shi, D. Yue, L. Zhang, J. Wang, H. Wang, C. Wang and D. Cui, *Chem. Eng. J.*, 2023, **461**, 142090.

55 M. V. Dinu, D. Humelnicu and M. M. Lazar, *Gels*, 2021, **7**, 116847.

56 K. Li, J. Yan, Y. Zhou, B. Li and X. Li, *J. Mol. Liq.*, 2021, **335**, 116291.

57 Z. Yin, C. Cui, H. Chen, K. Duoni, X. Yu and W. Qian, *Small*, 2020, **16**, 1902301.

58 H. Zhang, S. Zhu, J. Yang, A. Ma and W. Chen, *J. Membr. Sci.*, 2021, **636**, 119591.

59 J. Liu, J. Zhou, Z. Wu, X. Tian, X. An, Y. Zhang, G. Zhang, F. Deng, X. Meng and J. Qu, *J. Hazard. Mater.*, 2022, **432**, 128758.

60 Y. Jiang, B. Liu, J. Xu, K. Pan, H. Hou, J. Hu and J. Yang, *Carbohydr. Polym.*, 2018, **182**, 106–114.

61 Y. Liu, D. Wu, X. Wang, J. Yu and F. Li, *RSC Adv.*, 2018, **8**, 37715–37723.

62 H. Li, X. Cao, C. Zhang, Q. Yu, Z. Zhao, X. Niu, X. Sun, Y. Liu, L. Ma and Z. Li, *RSC Adv.*, 2017, **7**, 16273–16281.

63 B. Chen, F. Long, S. Chen, Y. Cao and X. Pan, *Chem. Eng. J.*, 2020, **385**, 123926.

64 B. Wang, B. Gao and Y. Wan, *Environ. Sci. Pollut. Res.*, 2019, **26**, 11535–11541.

65 M. E. Mahmoud, R. M. El-Sharkawy and G. A. A. Ibrahim, *J. Mol. Liq.*, 2022, **368**, 120676.

66 L.-Y. Guo, H.-Q. Lu, D. Rackemann, C. Shi, W. Li, K. Li and W. O. S. Doherty, *Chem. Eng. J.*, 2021, **416**, 129084.

67 X. Guo, Y. Liu and J. Wang, *J. Hazard. Mater.*, 2020, **400**, 123324.

68 N. E. Dávila-Guzmán, F. de Jesús Cerino-Córdova, E. Soto-Regalado, J. R. Rangel-Mendez, P. E. Díaz-Flores, M. T. Garza-Gonzalez and J. A. Loredo-Medrano, *Clean: Soil, Air, Water*, 2013, **41**, 557–564.

69 J. Wang and X. Guo, *Chemosphere*, 2022, **309**, 136732.

70 J. Wang and X. Guo, *J. Hazard. Mater.*, 2020, **390**, 122156.

71 E. Haque, J. W. Jun and S. H. Jhung, *J. Hazard. Mater.*, 2011, **185**, 507–511.

72 Y. Lv, J. Ma, K. Liu, Y. Jiang, G. Yang, Y. Liu, C. Lin, X. Ye, Y. Shi, M. Liu and L. Chen, *J. Hazard. Mater.*, 2021, **403**, 123666.

73 X. Wan, Z. Rong, K. Zhu and Y. Wu, *Int. J. Biol. Macromol.*, 2022, **222**, 725–735.

74 H. Li, V. L. Budarin, J. H. Clark, M. North and X. Wu, *J. Hazard. Mater.*, 2022, **436**, 129174.